Nuclear Engineering and Design/Fusion 2 (1985) 305–318
North-Holland, Amsterdam



# A COMPARISON OF PULSED AND STEADY-STATE TOKAMAK REACTOR BURN CYCLES. Part I: Thermal effects and lifetime limitations *

D.A. EHST, Y. CHA, A.M. HASSANEIN, S. MAJUMDAR, B. MISRA and H.C. STEVENS

*Fusion Power Program, Argonne National Laboratory, 9700 South Cass Avenue, Argonne, IL 60439, USA*

Received 16 April 1984

Four distinct operating modes have been proposed for tokamaks, and consequently a variety of thermal environments can be postulated for future reactor subsystems. Our study concentrates on lifetime limitations associated with fluctuating thermal loads on the first wall, limiter or divertor plates, and in the breeding blanket. Simultaneous failure from thermal fatigue, radiation damage, and disruption-induced erosion is considered, and burn length goals are calculated in order to help achieve high availability for a commercial reactor. In addition, the cost of thermal storage is found as a function of the dwell period between burns of a pulsed cycle; thermal storage is shown to be an expensive requirement for pulsed reactors.

## 1. Introduction

The tokamak was originally envisioned to provide the basis for a fusion reactor which would operate on a pulsed cycle. Design studies over the years have identified many perceived shortcomings for operation of a pulsed tokamak reactor. These issues are concerned with the costs of thermal and electric energy storage, thermal fatigue in the blanket, first wall, and other high temperature components, and mechanical fatigue associated with oscillating magnetic fields. There was a measure of enthusiasm, therefore, when it was recently discovered that tokamaks can be operated in a purely steady-state mode, via continuous wave (CW) RF heating and current drive. The STARFIRE tokamak study capitalized on the advantages of CW operation to demonstrate that such a fusion power plant could be economically competitive in producing electricity [1].

The principal concern with CW tokamak operation is the efficiency of generating the toroidal current by noninductive means. If a 10 MA toroidal current requires much more than 100 MW of auxiliary power absorbed in the plasma this may represent an unacceptable circulating power fraction and an unacceptably large capital cost for the driver. Unfortunately, experiments (e.g., PLT, Alcator C) are finding relatively small current generation efficiency for lower hybrid waves; scaling from present-day results, we would expect centrally peaked current density generation in a reactor with an efficiency, $\gamma$, of only $\sim 0.01$ A/W.

There are several proposals to improve this situation. Alternative drivers, such as the compressional Alfven wave, are theoretically superior to the lower hybrid wave, and may provide a large enough $\gamma$ to make CW operation attractive. Another suggestion is to use noninductive drive only during low density periods, when the ratio of current to driver power, $I_0/P_d$, is large. (For all noninductive drivers $I_0/P_d \propto \gamma/\bar{n}_e$, where $\bar{n}_e$ is the volume average electron density.) One possibility here is to use noninductive current drive during such periods of low density operation, driving the current above the minimum value needed for fusion operation, and then permitting the current, $I$, to decay resistively during a brief period of high density fusion operation until the cycle must be repeated. This mode [2–4], called internal transformer operation, completely eliminates the external transformer (i.e., the so-called ohmic heating coil). Also, a hybrid cycle has been proposed [2,5] in which $I$ remains constant, driven at high density during the fusion burn by an external transformer, and at low density by a noninductive driver while the transformer is reset.

These alternative modes of operation do, however, present fluctuating thermal loads on the reactor structure since fusion power varies with the changes in plasma density. Hence, many advantages of purely steady-state operation would be sacrificed. As the first

* Work supported by the US Department of Energy.

part of an extensive comparison of tokamak burn cycle options we report here on the effects of thermal fluctuations from pulsed cycles. We aim to determine reactor sensitivity to some uncertainties of plasma physics (pulse length, disruptions) as well as to choices among selected materials for reactor components. In this paper we consider the following reactor subsystems: first wall, limiter/divertor, breeder material, blanket structure, and thermal energy storage. A companion paper [6] deals with the effects of mechanical fatigue on magnetic systems, and presents a capital cost comparison for reactors with different burn cycles.

In section 2 we define the four burn cycles in more detail and identify operating windows for important factors such as thermal loads, burn periods, etc. Also the models used for the subsystems are presented. Much of the detailed subsystem analysis has already been documented in ref. [7] and we summarize only the salient conclusions in the present report. Specifically, in section 3 we discuss the implications of thermal fatigue on the performance of the first wall and limiter or divertor; goals for minimum fusion burn lengths are found. In section 4, where the thermal response of the blanket is explored, we find that the cost of thermal storage is a significant penalty for pulsed operation, and we point out the motivation to minimize the dwell period between fusion burns. We conclude in section 5 with some general observations as well as specific goals for tokamak research.

## 2. Models for burn cycle analysis

### 2.1. Reference reactor systems

Two basic tokamaks are considered in our study. The "7 m reactor" has a major radius $R_0 = 7.0$ and has a plasma quite similar to that in the STARFIRE reactor [1]. This device has a small "hole in the doughnut" and serves as a model for the continuous wave (CW) burn cycle. The second tokamak, the "8 m reactor," was selected to characterize burn cycles with inductive current drive. This tokamak, with $R_0 = 8.0$ m, is not an optimized design but is merely indicative of the size needed to obtain fusion burns $\gtrsim 10^3$ s by inductive means. Both tokamaks have comparable fusion power, $P_f \approx 4000$ MW, and neutron wall loads, $W_n \approx 4$ MW/m$^2$.

Considering first noninductive current drive, we recall [8] that, for fixed beta, $\beta_t$, and fusion power, operation at high average plasma temperature ($\bar{T}$) reduces the density and therefore decreases the required current drive power. However, the maximum toroidal magnetic field, $B_M$, must increase in order to keep $P_f$ constant. This tradeoff is explored in fig. 1 for the class of current drive techniques which add energy to electrons at suprathermal velocities. This "high-speed" drive is exemplified by lower-hybrid [9], magnetosonic [10], and electron cyclotron [11] waves and is characterized by an efficiency which scales as

$$I_0/P_d^{(0)} = \left(\gamma^{(0)}/n_{20}\right)(7.0\ \mathrm{m}/R_0),$$

where $n_{20}$ is $\bar{n}_e$ in units of $10^{20}$ m$^{-3}$. In the best theoretical case (relativistic limit) $\gamma^{(0)} \approx 0.2$ A/W, whereas present-day experiments [12,13] report $\gamma^{(0)} \approx 0.017$ A/W. From the figure we see driver power is minimized by operating at $\bar{T}_e \gtrsim 12$ keV; there is also great incentive to achieve $\gamma^{(0)} \gtrsim 0.1$ since driver power in excess of 200 MW will be an expensive item if driver cost exceeds ~ \$1/W. The net electric power is plotted

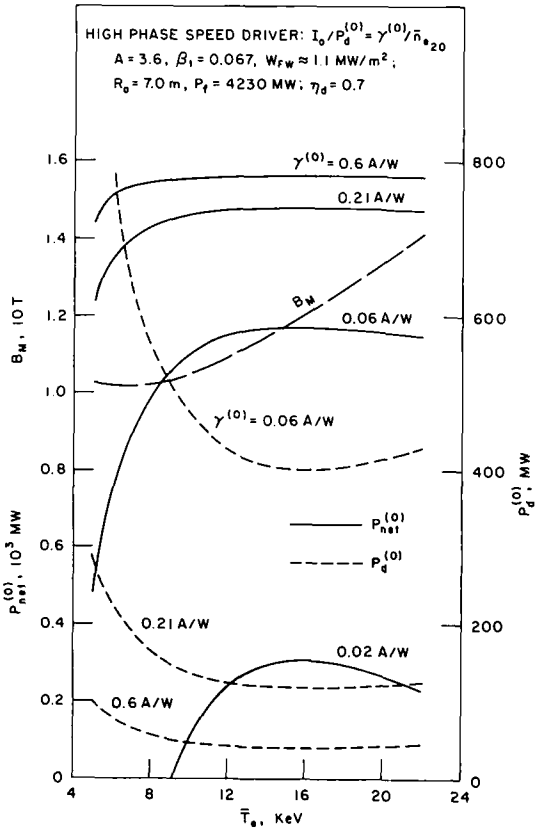


Fig. 1. High-speed current drive for various $\gamma^{(0)}$; required driver power, $P_d^{(0)}$, net electric output, $P_{net}^{(0)}$, and magnetic field, $B_M$, for $R_0 = 7.0$ m. Electric-to-current drive efficiency assumed to be $\eta_d = 0.7$.

from the approximate formula $P_{net} = 0.357P_{th} - 73$ MW $-(P_d^{(0)}/0.7)$, where the thermal power ($P_{th}$) is due to alpha heating ($P_\alpha$), the absorbed driver power ($P_d$), and neutron heating ($P_n$) with blanket enhancement: $P_{th} = P_\alpha + P_d^{(0)} + 1.14P_n$. Also, we note $P_{net}$ maximizes at $\bar{T}_e \gtrsim 12$ keV; $\gamma^{(0)} \gtrsim 0.06$ may suffice to achieve acceptable net power. The penalty for operation above ~ 12 keV is the rapid increase of $B_M$ above 11 T. The credibility and reliability of such very high field TF magnets is called to question.

Low speed wave drivers (Alfven) [10], ion cyclotron minority heating [14]) as well as neutral beams [15] are characterized by current drive which scales as

$$I_0/P_d^{(1)} = (\gamma^{(1)}/n_{20})(\bar{T}_e/10\text{ keV})(7.0\text{ m}/R_0),$$

where $\gamma^{(1)} = 0.16$ A/W in the best theoretical case [10]. The driver and net electric power are displayed in fig. 2 for low speed drivers. The goals for $\gamma$ ($\gtrsim 0.1$ A/W) and $\bar{T}_e$ ($\gtrsim 12$ keV) are the same as above. For our study we assume the maximum practical fields are those obtained in the STARFIRE design [1], $B_M = 11$ T, so we select $\bar{T}_e = 12$ keV as the operating point for the 7 m reactor.

The selection of an optimum operating temperature for an ohmically driven tokamak involves the issue of burn length. Assuming plasma resistance drops with $T_e$ we seek high temperature operation to maximize the burn length. However, the larger $B_M$ needed to keep $P_f$ constant as $T_e$ increases beyond ~ 8 keV implies larger plasma current, $I_0$, to maintain MHD equilibrium. In addition, plasma resistance $\propto Z_{eff}$. Hence the loop voltage scales as the product $I_0 Z_{eff}/\bar{T}_e^{3/2}$. For the 8 m reactor at constant $P_f$ we find this factor decreases rapidly until $\bar{T}_e \gtrsim 12$ keV and only slowly at higher $\bar{T}_e$. Countering this drop in loop voltage is a decrease in volt-seconds stored in the transformer of the reactor. At higher $T_e$ the toroidal field coils (TFC) become thicker since $B_M$ is getting larger. The result is a reduction in the size of the hole in the doughnut, $R_{OH}$, and in the transformer flux, $\Delta\phi_{OH,p} = \pi R_{OH}^2 \Delta B_{OH}$.

If we assume a transformer with field swing $\Delta B_{OH} = 2 \times 10$ T and a resistance close to Spitzer [6]

$$R_{SP} = 2.2n\Omega \times Z_{eff}(10\text{ keV}/\bar{T}_e)^{3/2},$$

we find that the burn length, $t_f$, has a broad maximum, nearly $10^4$ s, for $8 \lesssim \bar{T}_e \lesssim 16$ keV. In order to reduce the demands on the TFC we choose to operate at the lower end of this range, where $B_M$ is relatively small. Our reference design operates at $\bar{T}_e = 10$ keV with $B_M = 9.8$ T, substantially lower than for the 7 m tokamak. Table 1 provides additional parameters of the two reference reactors.

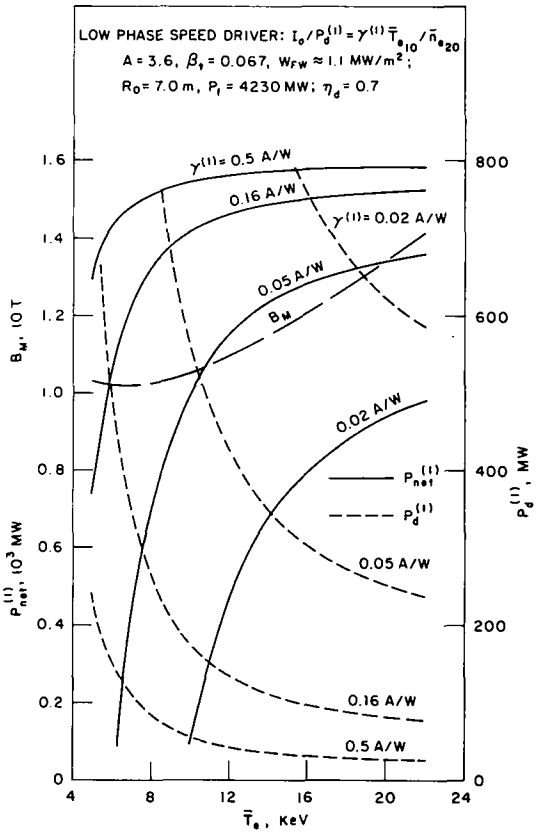


Fig. 2. Low-speed current drive for various $\gamma^{(1)}$.

### 2.2. Reference burn cycles

– Conventional ohmically driven (OH) cycle. This cycle is shown schematically in fig. 3. The toroidal current is driven by a transformer, and once the volt-seconds are consumed the current decays and the fusion burn is extinguished. Both the current pulse, $t_1$, and fusion power period, $t_f$, are the same, ~ $10^3$–$10^4$ s. Thermal loads and magnetic fields oscillate with the same periodicity. The figure illustrates single swing transformer action (plasma current and equilibrium field always in one direction), but double swing operation may be more attractive. Neutron power, $P_n$, and fusion thermal power, $P_\alpha$, are zero when the plasma density and temperature drop; during this down period, thermal power must be extracted from auxiliary storage units to supply the steam generators. Previous studies [16–18] of the OH cycle have addressed some issues related to the burn length. We shall see in section 3.3 that the burn period of the OH cycle may be too short to avoid

Table 1
Reference tokamak reactors

| Parameter | 8 m reactor | 7 m reactor |
|---|---|---|
| Aspect ratio, $A$ | 4.0 | 3.6 |
| Elongation, $\kappa$ | 1.6 | 1.6 |
| Triangularity, $d$ | 0.2 | 0.2 |
| Average beta, $\beta_t = 0.24/A$ | 0.060 | 0.067 |
| Safety factor, $q_{axis} - q_{lim}$ | 1.0–2.5 | 1.0–2.5 |
| Major radius, $R_0$ | 8.0 m | 7.0 m |
| Inboard blanket/shield/scapeoff, $\Delta'$ | 1.4 m | 1.4 m |
| Maximum field at TFC, $B_M$ | 9.81 T | 11.2 T |
| Field at $R_0$, $B_0$ | 5.64 T | 5.85 T |
| Toroidal current, $I_0$ | 13.0 MA | 14.8 MA |
| Electron (ion) temperature, $\bar{T}_e$ ($\bar{T}_i$) | 10.0 keV (10.9 keV) | 12.0 keV (13.9 keV) |
| Electron density, $\bar{n}_e$ | $2.02 \times 10^{20}$ m$^{-3}$ | $1.90 \times 10^{20}$ m$^{-3}$ |
| Tritium density, $\bar{n}_T (= \bar{n}_D)$ | $0.719 \times 10^{20}$ m$^{-3}$ | $0.696 \times 10^{20}$ m$^{-3}$ |
| Effective ion charge, $Z_{eff}$ | 1.70 | 1.80 |
| Fusion power, $P_f$ | 3900 MW | 4230 MW |
| Neutron power, $P_n$ | 3120 MW | 3380 MW |
| Alpha power, $P_\alpha$ | 780 MW | 846 MW |
| First wall thermal (photon) power, $P_{FW}$ | 687 MW | 704 MW |
| Current drive power (typical), $P_d$ | 0 MW | 150 MW |
| Neutron wall load, $W_n$ | 3.5 MW/m$^2$ | 4.4 MW/m$^2$ |
| Thermal power, $P_{th} = 1.14P_n + P_\alpha + P_d$ | 4337 MW | 4849 MW |
| Gross power (100% D.F.), $P_g = 0.357\,(P_{th} + 33$ MW) | 1560 MW | 1743 MW |
| Net power (nominal), $P_{net} = P_g - 85$ MW $- (P_d/0.5)$ | 1475 MW | 1356 MW |
| Plasma self-inductance, $L$ | 17.2 $\mu$H | 14.1 $\mu$H |
| Spitzer toroidal resistance, $R_{SP}$ | 3.69 n$\Omega$ | 2.74 n$\Omega$ |

serious damage from thermal effects.

– Continuous wave (CW) operation. This technique [1,19] is only practical if noninductive current drive is efficient enough during high density fusion operation that the circulating power, $P_d$, is a small fraction of the fusion power. With this proviso, however, reactor operation is possible in principle for very long periods (months), with shutdown dictated only by needs for reactor maintenance. Fatigue is expected to be of minor concern since only a few hundred thermal and magnetic cycles occur in the reactor lifetime. Thermal storage is eliminated, slow current and power ramps minimize the cost of startup power supplies, disruptions may be very infrequent, and additional design latitude derives from eliminating the external transformer.

– Internal transformer (IT) operation. This mode of operation [2–4] requires no external transformer. Instead, noninductive current drive is used during periodic low density phases to boost toroidal current by a small increment $\Delta I$ (see fig. 4). Between current drive periods the density is increased for full fusion power production, and the current decreases resistively for a burn length $t_f \approx \Delta t_1 \approx (\Delta I/I_0)(L/R)$. If we keep the toroidal current nearly constant ($\Delta I \ll I_0$), the burn is limited to a relatively short period ($\sim 10^2$ s), and this mode will result in many times more total fusion cycles in the reactor lifetime than the OH cycle. The fusion power oscillations lead to thermal cycling, as in the OH cycle. The equilibrium field, $B_{EF}$, will also fluctuate; even though toroidal current is nearly steady, poloidal beta, $\beta_p$, fluctuates from density cycling. We can expect $B_{EF}$ variations on the order of half the full field value, for a typical IT cycle.

– Hybrid transformer operation. A variation of the IT cycle, this would use an external transformer (OHC) to maintain $I_0$ during the fusion burn and then keep $I_0$ at full value with low density noninductive current drive while the transformer is quickly recharged [2,5]. As with the IT, both thermal and magnetic fluctuations occur, but the fusion period is much longer than the IT cycle,

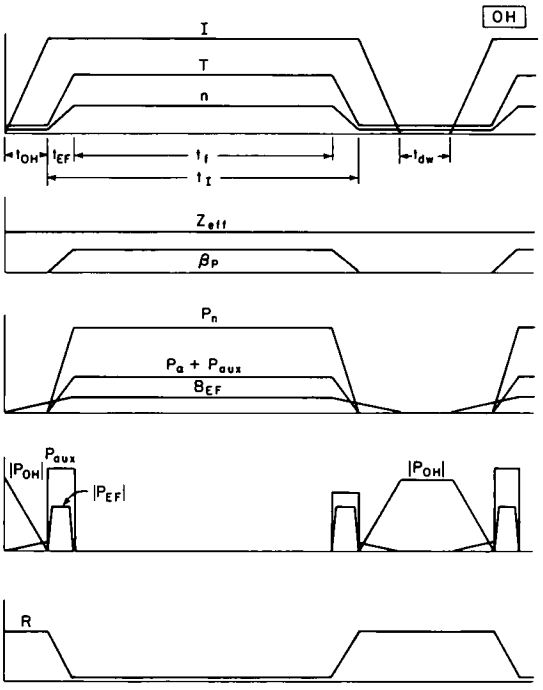


Fig. 3. Schematic OH cycle. Auxiliary power, $P_{aux}$, is used for heating to ignition during period $t_{EF}$. Startup and shutdown ramps are nearly symmetric.

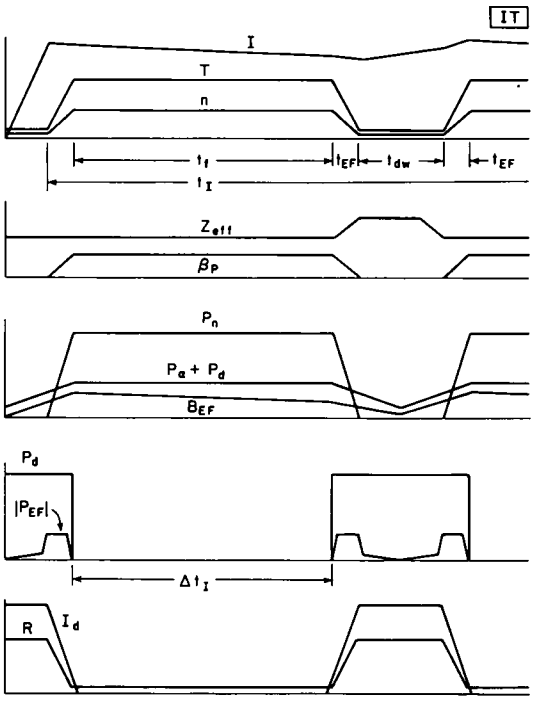


Fig. 4. Schematic internal transformer cycle. Driver power, $P_d$, is used only during dwell, $t_{dw}$, to increase toroidal current, $I$; plasma resistance, $R$, is made to increase during dwell by enhancing $Z_{eff}$.

resulting in fewer lifetime cycles. Compared to the OH cycle this mode benefits from keeping $I_0$ constant: equilibrium field power, $P_{EF}$, may be smaller, downtime may be shorter, periodic purging and plasma breakdown is avoided, and disruptive regimes might be circumvented. The burn cycle wave forms are similar to those in fig. 4, except that the toroidal current remains constant (for many months, in principle) and with the addition of a power supply ($P_{OH}$) which charges the OHC during the dwell period. As with the OH and IT burn cycles, hybrid operation is sensitive to thermal cycling damage (section 3) and requires expensive thermal storage (section 4) during the dwell period.

### 2.3. Subsystem models and performance analysis

For our studies we consider multiple concepts for most subsystems in order to reflect the uncertainty of future technology.

In the case of the limiter structure we have studied two basic alternatives. One system, representative of near-term technology, has a copper alloy for the heat sink structure and is water cooled (4 MPa, 130°C). A more advanced alternative has a vanadium alloy heat sink with liquid lithium coolant (4 MPa, 210°C). The limiter geometry is that proposed and analyzed in the STARFIRE study [1]. The front face of the limiter (that portion closest to the plasma) is modeled as a flat slab with a thermal load, $W_{ff} = 1.5$–$3.5$ MW/m$^2$, and the leading edge is analyzed as a cylinder. Careful design of the limiter geometry is expected to result in leading edge thermal loads smaller than those on the front face; we consider $W_{le} = 0.75$–$1.75$ MW/m$^2$. For this study we assume the entire limiter is laminated with a surface material (tiles) specifically designed to reduce sputtering contamination of the plasma [20]. The high plasma temperature at the front face constrains our choice to a small class of options, and we pick beryllium as a typical coating. Near the leading edge the plasma temperature is lower, and a larger number of options are possible, and we consider both beryllium and tungsten as coatings.

The first wall is treated as a simple bank of cooling tubes [21]. One option is water cooled (15 MPa, 300°C)

with prime candidate alloy (PCA) for the tube structure. We use 20% cold worked 316 stainless steel to model the PCA properties. At these high pressures a thin wall tube requires a small inner radius, and we consider $r_i = 3$–$10$ mm. The more advanced design utilizes liquid lithium (2 MPa, 350°G) as a coolant and vanadium as the structure. The low pressure permits relatively large radius piping; $r_i = 25$ cm is chosen. The surface heat load $W_{FW} = 0.5$–$1.0$ MW/m$^2$, is due mainly to photon radiation, so the first wall is taken to be bare structure.

Fatigue damage to reactor structure arises from variations in thermal expansion. Thin structures and cooling tubes designed for high static primary pressures are analyzed with smooth sample data curves which show the number of cycles to crack initiation, $N_f$, versus the total strain variation per cycle. For the duplex limiter geometry, fatigue is not life limiting to the coating since cracking on the surface will not appreciably degrade the limiter's function. However, the thermal stresses imposed on the substrate will depend strongly on the geometry of the protective beryllium or tungsten tiles which are bonded to the heat sink, and fatigue failure of this structural component cannot be tolerated. Details of the methods of stress analysis are given in ref. [20].

Besides thermal fatigue, the first wall and limiter experience high heat loads, and, based on previous fusion materials studies [20,22,23], appropriate temperature limits have been imposed for the various coatings and heat sinks. These constraints reflect the life-limiting effects of high temperatures on radiation-induced swelling, tensile strength, ductility, and thermal creep. Another life limit to plasma-exposed components is the thermal damage from major disruptions. The primary parameters are the energy deposition per unit area, the thermal dump duration, and the frequency of disruptions. Extrapolating from INTOR [20] we expect maximum energy densities of $\sim 800$ J/cm$^2$ on the first wall and $\sim 2500$ J/cm$^2$ on the limiter. The resulting vaporization and melt layer thickness are found for the candidate materials using the A*THERMAL code [24] for several disruption times. For this burn cycle study we have adopted one particular model for the frequency of disruptions, namely, that their occurrence correlates with the number of fusion burn cycles. (This is expected if disruptions are initiated by transient plasma conditions, such as current density and pressure profiles.) Thus the prevalence of disruptions is treated statistically, and we examine probabilities of $f = 10^{-2}$, $10^{-3}$, and $10^{-4}$ disruptions per burn cycle.

Radiation effects are included as follows. The first wall heat load (mostly photons) is $W_{FW} \approx W_n/4$, the limiter's leading edge experiences $W_{le} \approx 0.4\ W_n$, and the front face has $W_{ff} \approx 0.8\ W_n$, where $W_n$ is the neutron wall load. In the thermal analysis of coatings and structure nuclear bulk heating is included. Based on a survey of swelling and loss of ductility under radiation conditions we assign these life limits, $L_{rad}$, for neutron fluence to structural materials: Cu = 4 MW · yr/m$^2$; PCA = 12 MW · yr/m$^2$; V = 24 MW · yr/m$^2$. Radiation-induced creep is felt to be less damaging than thermal creep, and values as high as 5% are assumed acceptable in our stress analysis. (Further discussion of thermal and radiation creep is given in refs. [7] and [22].)

The total number of fusion cycles in the reactor lifetime is based on a 40 years assumed lifetime and 80% availability ($1.0 \times 10^9$ s of operation). Our philosophy is that all burn cycles must achieve this high availability to be of interest to a utility. We attempt to calculate burn cycle requirements needed to approach these goals. An accurate estimate of subsystem reliability, mean time to replace failed components, and system availability is obviously not possible at present. However, the data presented here provide a useful comparison of the relative attractiveness of the various burn cycles to different reactor subsystems.

## 3. First wall and limiter lifetime

Our aim is to maximize component lifetime against simultaneous failure modes. First, thermal fatigue is calculated, and we find that cycle life generally decreases for thicker structures and coatings. Next we study material loss from disruptions and show how component cycle life increases with thicker structures and coatings. The component dimension corresponding to the intersection of these life curves is considered optimum for obtaining the longest cyclic life. Then the minimum fusion burn length is found such that the total cyclic life is not shorter than the expected component life against radiation damage. (Erosion due to sputtering is not extensively examined as a life limit; we assume that net sputtering erosion must be made insignificant either through proper plasma edge conditions or, for example, via periodic resurfacing techniques.)

### *3.1. Thermal fatigue*

A thermal hydraulics analysis was done to provide temperature distributions in the coatings and structural materials. These results are used as input to the stress analysis and to ascertain that temperatures are within the acceptable levels. One-dimensional steady-state calculations are performed. We find that, for a given

heat sink thickness in the limiter, surface temperatures increase with the thickness of the coatings as well as with the thermal heat load, as expected. The leading edge, due to its cylindrical geometry, experiences rising temperatures also in the heat sink as the coating thickness increases [20].

For design purposes a safety factor of two on strain or twenty on cycles is applied to the fatigue crack initiation curves of the various structural materials [7]. As an example, fig. 5 shows the fatigue life of beryllium-clad copper as a function of the coating thickness and surface heat flux at the leading edge. In general, the fatigue life decreases with increasing coating thickness and increasing surface heat flux. Beryllium-coated copper has a longer life than tungsten-coated copper. For small coating thicknesses ($\lesssim 1$ cm), the use of a stronger copper alloy (e.g., AMAX-MZC) instead of pure annealed copper can increase the design fatigue life significantly. For the alternative heat sink alloy (V–15Cr–5Ti), we find, in general, the fatigue life of vanadium is much greater than for copper. Except for small coating thicknesses ($\lesssim 2$ mm), beryllium-coated vanadium has a longer fatigue life than tungsten-coated vanadium.

The top surface of the limiter is analyzed as a flat plate constrained by the colder back part of the limiter. The fatigue life of both copper and vanadium heat sinks, as functions of beryllium coating thickness and surface heat flux, was calculated. Despite higher surface heat loading, the cyclic life of the top surface is comparable to that of the leading edge.

Fig. 6 shows the plot of cyclic life versus first wall tube thickness, $\delta$, for various thermal wall loads on a tube of 316 stainless steel with an inner radius of 5 mm. Also shown in this figure (by open circles) are the maximum thicknesses corresponding to a maximum allowable metal temperature of 500°C. The fatigue curves and the maximum temperature limit give upper bounds to wall thickness for a given surface heat flux. A lower bound for the wall thickness is set by the primary stress criterion, $P_m \lesssim S_{mt}$. The figure shows the minimum thickness corresponding to a time-dependent stress limit

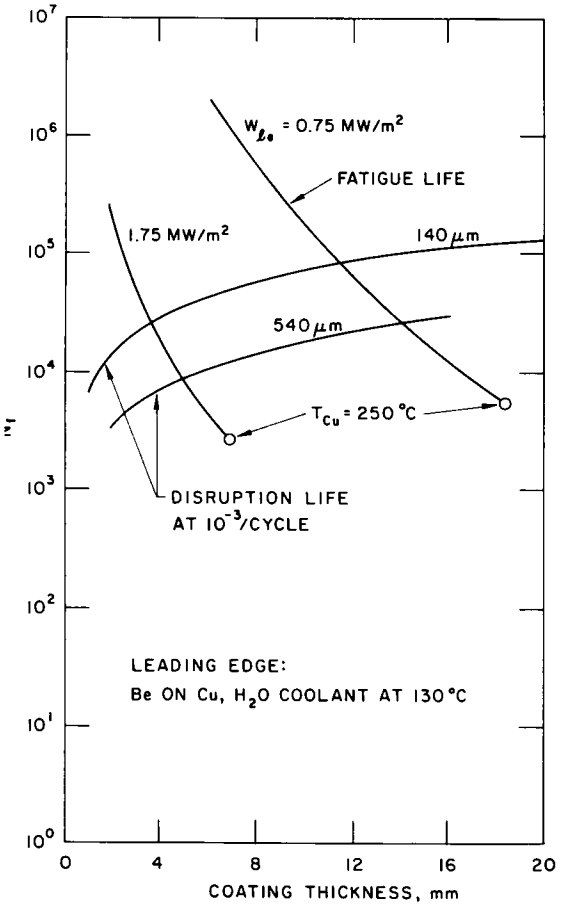


Fig. 5. Leading edge cyclic life versus fatigue and disruption erosion; open circles indicate thermal limit for copper above which structural characteristics deteriorate.

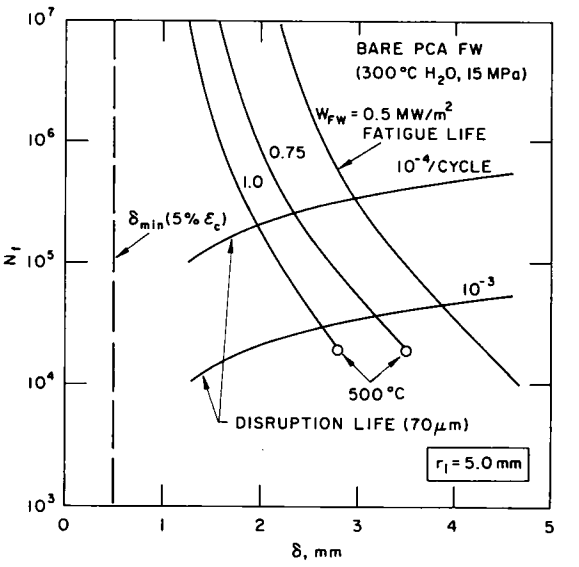


Fig. 6. First wall cyclic life versus fatigue and disruption erosion; minimum pipe thickness to withstand rupture, $\delta_{min}$, is set by 5% radiation-induced creep strain. Open circles correspond to temperature above which thermal creep is unacceptably large.

$S_{mt}$ corresponding to a maximum radiation-induced creep strain of 5%. The difference between the lower bound and the upper bound for thickness may be considered as the margin against erosion.

Similar plots were made for the case of V-15Cr-5Ti with a tube of radius 25 cm. In this case the maximum metal temperature limit of 600°C sets an upper bound for the vanadium first wall thickness. Because of their superior thermal properties vanadium tubes can have significantly larger wall thickness (6–10 mm) and longer cyclic lifetime ($N_f \gg 10^6$) than 316 stainless steel tubes.

### 3.2. Erosion from disruptions

Fig. 7 shows the total material erosion as a function of disruption energy density for both first wall and limiter materials. Vanadium as a first wall material results in much less erosion than stainless steel. At these energies the main material erosion is from melting. For limiter coatings, beryllium shows much higher erosion than tungsten. The threshold energy density to induce melting in beryllium is near 350 J/cm$^2$ while for tungsten it is about five times higher. This is mainly because of the very high melting point of tungsten.

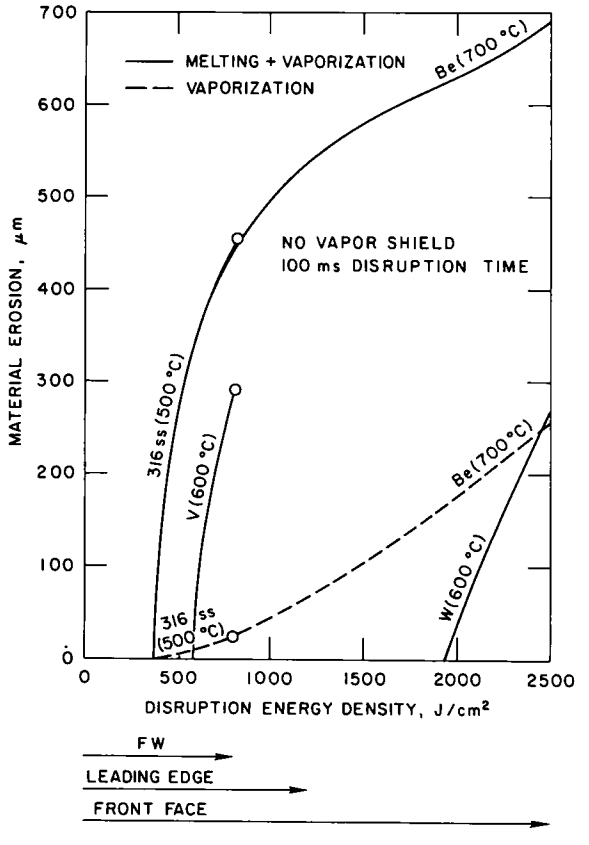


Fig. 7. Disruption damage. Bare steel or vanadium are not considered for the limiter surface.

Note that the material loss is quite sensitive to the energy density. If steps can be taken to reduce disruption energy densities by a factor of two from the worst cases shown, then significant reductions in damage can result. Likewise, if the melt layer is stable and only vaporized material is actually lost, then erosion can be less significant.

### 3.3. Lifetime analysis and burn goals

We begin by considering the limiter's leading edge, and we first consider the copper heat sink with water coolant and a beryllium coating (fig. 5). As previously stated, fatigue increases with thinner coatings. However, thinner coatings are more easily eroded by repeated disruptions. From fig. 7 we might expect up to 540 $\mu$m of beryllium removal per disruption near the upper limits of leading edge thermal dumps ($\sim$ 1000 J/cm$^2$). Hence the beryllium coating, with thickness $\delta_{Be}$, can be removed in the worst case after a number of fusion cycles $N_f = \delta_{Be}(f \times 0.54\ \text{mm})^{-1}$, where $f$ is the average frequency (probability) of disruptions per burn cycle. Fig. 5 displays $N_f$ versus $\delta_{Be}$ for $f = 10^{-3}$ (one disruption per thousand burn cycles) and two different coating removal rates. The optimum coating thickness is the intersection of fatigue and disruption curves. For example, for high leading edge heating, 1.75 MW/m$^2$, and mild disruption damage, 140 $\mu$m lost per disruption, the maximum lifetime is to be expected for $\delta_{Be} = 3.6$ mm, which results in a survival time of $N_f = 2.7 \times 10^4$ burn cycles.

Finally, we fold into our analysis the radiation life limit for the heat sink. Our philosophy is that the fusion burn length, $t_f$, should be long enough that the cycle life, $N_f$, is at least as long as the radiation life. Thus, we compute the minimum

$$t_f = \frac{L_{rad}}{W_n N_f} - 100\ \text{s},$$

where we assume a 100 s lapse between burns. As an illustration, the copper heat sink is believed to have poor radiation resistance, $L_{rad} \approx 4$ MW · yr/m$^2$; at a neutron wall load of $W_n = 4$ MW/m$^2$ one might expect to require its replacement every year. Then, a fusion period $t_f = 1.1 \times 10^3$ s would be needed in order for a cyclic lifetime $N_f = 2.7 \times 10^4$ to equal the radiation lifetime. Fig. 8 shows these burn goals for the beryl-

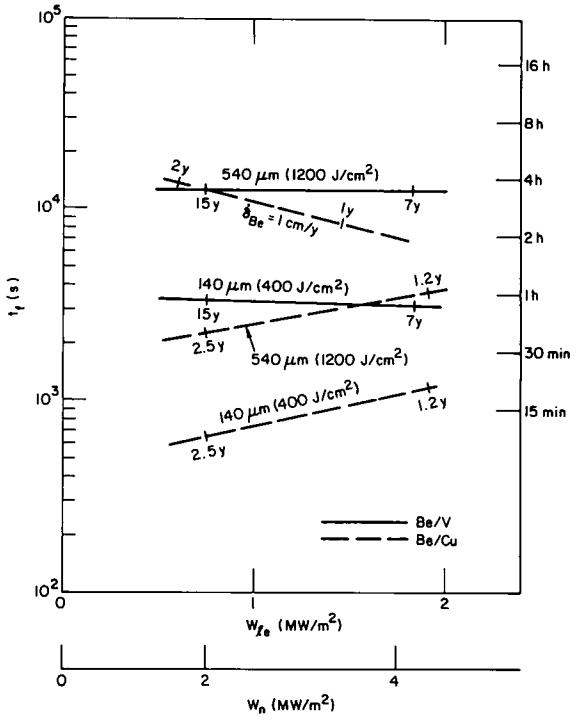


Fig. 8. Fusion burn length goals to maximize limiter's leading edge life against fatigue, disruptions, radiation and sputtering. Disruption frequency is assumed to be $f = 10^{-3}$ disruptions/cycle with no net sputtering, except for $\dot{\delta}_{Be} = 1$ cm/yr sputtering curve, which assumes $f \equiv 0$. Component replacement interval is indicated along the curves.

lium/copper leading edge under different conditions. In the case of severe disruption damage there is a strong motivation to achieve $t_f \approx 1$ h. The motivation for long burns diminishes for more mild disruptions. In fact, according to fig. 7, disruptions do no damage at thermal loads $\lesssim 300$ J/cm$^2$, so very thin coatings with negligible fatigue could be selected in this limit. The first lesson we have learned is that $t_f \approx 1$ h may be adequately long to eliminate fatigue as a life-limiting consideration if the limiter leading edge has a heat sink with poor radiation resistance. At 80% availability we note the limiter calendar lifetime is $T = L_{rad}/(W_n \times 0.8)$. $T$ is indicated by the tick marks on the curves in fig. 8 and is relatively short ($\sim$ 1–2 yr) for the copper structure.

It may well be that a commercial reactor would be designed with more radiation resistant materials in order to extend the period between limiter repairs. As an example we consider a vanadium heat sink at the leading edge, clad with beryllium. The superior fatigue resistance of vanadium results in a much longer cyclic life than the copper heat sink. For moderate damage rates, disruptions are the life-limiting concern, so $\delta_{Be}$ should be maximized to the temperature limit. The corresponding number of burn cycles can again be converted to a burn length such that the cycle lifetime at least equals the radiation lifetime. For vanadium, however, radiation resistance is believed to be much better than for copper (we take $L_{rad} = 24$ MW · yr/m$^2$). The results are shown in fig. 8. Compared to a copper heat sink there is strong motivation to achieve longer burns. For severe disruptions burn times exceeding 3 h are desired. These longer burns are needed in order to achieve the full potential radiation life of the limiter, in the range of seven to fifteen years.

In the desirable situation where disruptions can be completely eliminated from tokamak reactors we must consider sputtering as an erosion mechanism. In fig. 8 we illustrate the burn cycle implications with $\dot{\delta}_{Be} = 1$ cm/yr. Since sputtering life is so short, radiation damage does not concern us in this limit. The beryllium coating is increased to the temperature limit to maximize life against erosion, and the number of acceptable fatigue cycles is found. For the copper heat sink $N_f$ is now smaller than for the cases dominated by disruptions so a longer $t_f$ ($\gtrsim 3$ h) is needed to obtain a 1–2 yr lifetime of the leading edge; for the vanadium substrate $N_f$ is now larger, so a shorter $t_f$ ($\lesssim 100$ s) is permissible.

Tungsten has also been proposed as a limiter coating at the leading edge. If the plasma temperature exceeds $\sim$ 50 eV at the leading edge the high net sputtering of tungsten may preclude its use [25]. However, at lower temperatures net sputtering is quite low. In addition, disruptions do little damage to a tungsten coating, at the leading edge; see fig. 7. Hence, at such low temperatures erosion may not be significant for tungsten coatings. A thin tungsten cladding, $\delta_W$, would be specified. Since our fatigue calculations show very large cycle lifetimes for either copper or vanadium substrates with $\delta_W \lesssim 1$ mm we find that fatigue may not be an issue for the leading edge whenever a tungsten cladding can be used.

An identical lifetime analysis was done for the front face of the limiter. Typical results for moderate and severe disruptions are displayed in fig. 9. Our first observation is that $t_f \approx 1$ h is adequate for the front face with a copper heat sink, even with the worst disruption damage. However, the one- to two-year radiation life of copper is so short that there will be great incentive to consider materials such as vanadium. Then we find, in order to achieve the six-fold increase in limiter life, the burn length must be extended so as not to aggravate the

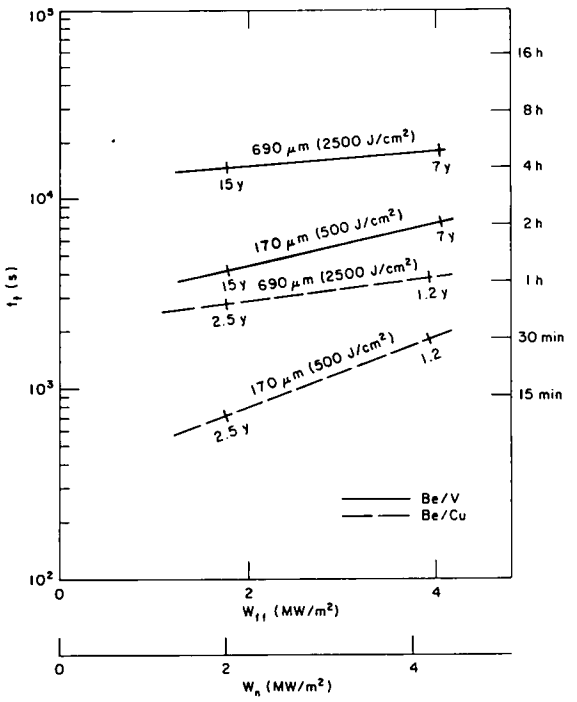


Fig. 9. Fusion burn goals to equate cyclic and radiation life of limiter's front face; no sputtering; $f = 10^{-3}$ disruptions/cycle.

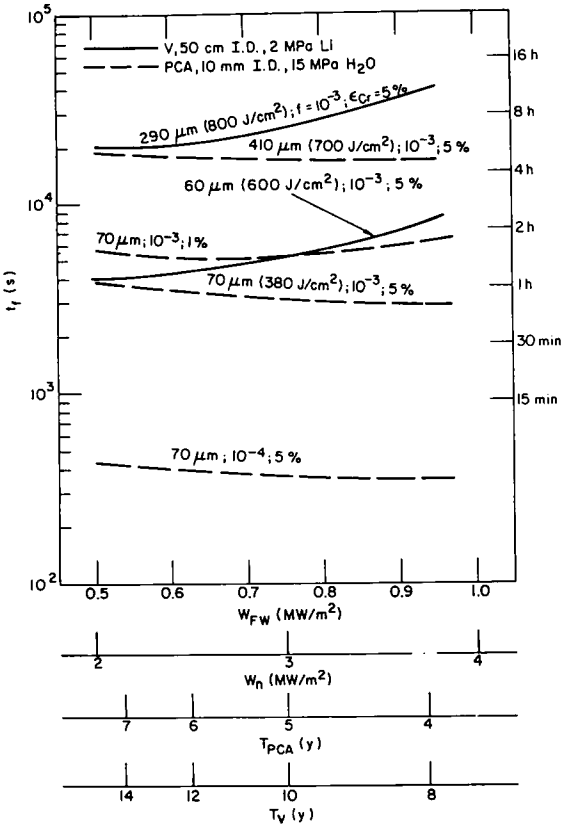


Fig. 10. Fusion burn goals to equate cyclic and radiation life of first wall; sputtering is negligible. Component replacement interval is given by lower abscissas.

fatigue problem. For moderate disruptions we need $t_f \sim 1$–2 h. Of course, if the frequency of disruptions were $f \ll 10^{-3}$ then thinner beryllium coatings, with resulting longer fatigue life for the substrate, would be appropriate. In the extreme where sputtering erosion limits the lifetime to ~ 1 to 2 yr the burn length would need to be only 15–30 min in order to eliminate thermal fatigue as a concern with a vanadium substrate.

We next analyze the first wall lifetime, starting with the bare PCA water-cooled tubes. In fig. 6 we display the cycle lifetime against disruptions for $f = 10^{-3}$ and $10^{-4}$, assuming modest thermal energies in the disruption (380 J/cm² removing 70 μm of PCA). The tubing is assumed to fail shortly after disruptions thin the wall to $\delta_{min}$. (For $\delta < \delta_{min}$ the stress will result in creep in excess of 5% at 100 dpa.) As with the limiter we compute the fusion burn period needed for the cycle lifetime to equal the radiation life (with $L_{rad} = 12$ MW · yr/m²). The results, shown in fig. 10, indicate that relatively short burns, $t_f = 1$ h, suffice to eliminate the cycling factor from concern when there are infrequent or mild disruptions. It is conceivable that the disruption damage could be more troublesome, however. Merely increasing the energy deposition from 380 to 700 J/cm² multiplies the melting and vaporization loss by a factor of six for PCA (see fig. 7). This motivates a design goal for much longer fusion burns; as shown in fig. 10, $t_f \approx 5$ h is needed to realize the full radiation life potential in this case.

Finally, we consider the burn goals needed to achieve the full benefits of radiation resistant structure such as vanadium. The 600°C thermal creep limit on vanadium [22] constrains $\delta_V$ to $\lesssim 10$ mm, and we find disruption erosion dominates fatigue as a consideration. Our results, displayed in fig. 10, show that $t_f$ may be as long as that required for the PCA first wall in order to achieve twice the in-reactor lifetime (8–14 yr versus 4–7 yr). In the pessimistic disruption scenario depicted we find $t_f \approx 8$ h is desirable at high wall loads.

We close this section with some general observations. Our results typically show that "near-term" structures

such as copper limiters and a steel first wall can tolerate relatively short fusion burns because their radiation life is thought to be short. In order to take full advantage of advanced materials with longer radiation life it will be necessary to arrange for longer burns (CW or long pulse operation). On the other hand, reactors with short burns ($t_f \sim 100$ s), operating in the internal transformer mode, will not be attractive unless the disruption frequency is $f \lesssim 10^{-5}$ and sputtering erosion ($\dot{\delta}$) is $\lesssim 1$ cm/yr.

Generally speaking, the higher thermal loads are more demanding on our designs. In the first place this is because we have assumed the higher thermal loads are associated with higher neutron damage and therefore shorter in-reactor life. In the second place these higher thermal loads exacerbate the fatigue problem and generally require longer burns in order to not surpass the limit on cycle lifetime.

Finally, we caution that our results only display general trends. Reactor availability should improve with several factors: use of more radiation and fatigue resistant materials; reduction in the frequency and severity of disruptions; reduction in net sputtering erosion; selection of disruption resistant materials; operation at lower wall loads; as well as operation with longer fusion burns.

## 4. Blanket thermal effects and thermal energy storage

Of two viable breeding blankets studied, one with a solid breeder and water coolant and one with self-cooled liquid lithium, only the former is investigated with a detailed burn cycle analysis [7]. We consider a model burn cycle with 1 h burn, 10 s linear power decrease, and a variable dwell period, $t_{dw}$, followed by a 10 s power increase. Explicit blanket temperature variations are calculated for four cases which span the expected dwell periods for the OH, IT, and hybrid cycles (section 2): $t_{dw} = 0$, 30, 90, 200 s. During the burn the wall load is set at $W_n = 3.45$ MW/m$^2$.

The solid breeder blanket contains $Li_2O$ granules and is punctuated by ten rows of cooling tubes designed to maintain (steady-state) temperatures between 410°C and 800°C in the breeder. Coolant inlet/outlet temperature is 280°C/320°C. Experience shows that an acceptable assessment of this system can be carried out with results based on only three representative blanket regions. We calculate the transient temperature response near the first wall (100% of the nuclear power density, 41 W/cm$^3$), at the 25% power region, and at the back of the blanket (5% power). Since the volume of the blanket region associated with each coolant channel in an exponentially decreasing nuclear power field increases as the blanket regions are located further away from the first wall, the thermal inertia of regions in the radial direction (depthwise) increases. Our results agree rather well with a simple model proposed by Deis [26]. As expected, the changes in the coolant outlet temperatures and temperature gradients in the $Li_2O$ blanket increase as the dwell times increase. If the dwell times are sufficiently long ($\gtrsim 200$ s), the temperatures of components are found to decrease to the coolant inlet values.

Thermomechanical fatigue may not be critical to the porous $Li_2O$ mass, which is fabricated at only 85% of theoretical density. Cooldown of the breeder below its lower operating limit can affect tritium recovery, but this may be unimportant if the duty factor is high. Thermal stresses across the coolant tubes during power transients ($< 5$ MPa) are much less than the primary stress ($\sim 55$ MPa) due to the high pressure coolant (at 15 MPa) so fatigue is insignificant. Dimensional changes are possible at the breeder/cooling tube interface after cyclic operation. Although this could adversely affect the thermal conductance at the interface it might be controlled with a metal felt sleeve around the tube. In all, no severe degradation of the blanket life is anticipated due to cyclic operation.

Although, due to their lower thermal inertia, the high power blanket regions have faster time response and larger temperature fluctuations than the low power regions, these differences are averaged as the water flows from the cooling tubes and is mixed in the headers leading to the steam generators. Fig. 11 displays the mixed coolant temperature for one case, $t_{dw} = 30$ s. Note the temperature drops steadily for 40 s to 304°C but requires several minutes to recover once nuclear heating returns. Even for $t_{dw} = 0$ s (10 s power drop followed by an immediate power increase), the limiting case for IT operation, the coolant drops to 313°C. Since the electric power is proportional to coolant temperature rise in the blanket, we find the generator output drops transiently to $(313 - 280)/(320 - 280) = 83\%$ of its steady state rating even with this shortest dwell. Moreover, the whole power conversion system [1] is based on coolant outlet temperatures of 320°C which generate slightly saturated steam (299°C at 6.3 MPa), so coolant temperatures below $\sim 300$°C result in wet steam at 279°C entering the turbine. Both steam temperature fluctuations and moisture content are damaging to the turbine blades, but this may not be critical if the burn cycle's duty factor is very high. We assume the dominant concern is the transient electric output of the fusion power plant. Hence, we must provide an energy storage system which supplies the whole energy deficit

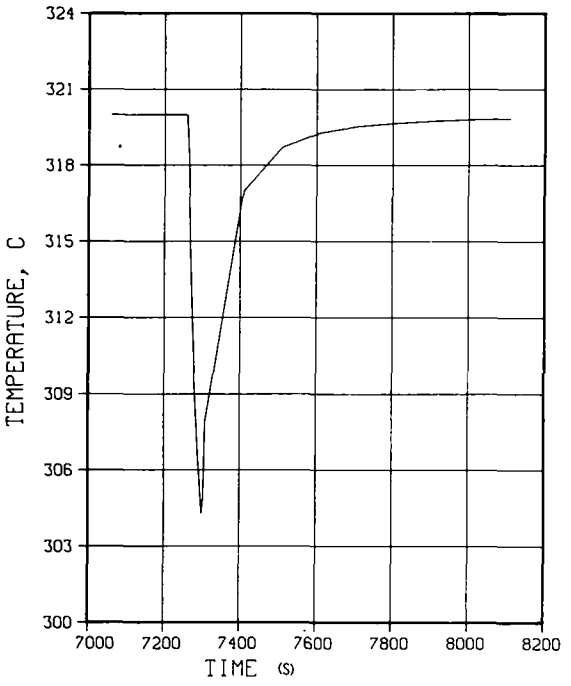


Fig. 11. Volumetric average temperature response: 30 s dwell.

during the dwell with a fast time response to keep the electric power constant.

For a 4000 MW thermal reactor, the energy deficit varies from 40 GJ to over 800 GJ as $t_{dw}$ varies from 0 to 200 s. Several thermal storage systems, such as packed columns of metals or ceramics, and chemicals, were considered for energy storage. However, they did not appear to be practical if the thermal energy is to be withdrawn in a relatively short period of time. Energy storage in pressurized water, which can be withdrawn as steam by flashing [27], or energy storage in a high temperature liquid metal which can be fed into a heat exchanger/evaporator unit appear to be practical, although such systems are considered to be at the limit of existing technology. Analyses show that a pressurized water/steam system is suitable for the solid breeder blanket, and a hot sodium reservoir would be practical for the liquid lithium blanket. A detailed description of the two systems is available in ref. [7], and the component costs are summarized in tables 2 and 3.

In comparing burn cycles (as, for example, in ref. [6]) we base thermal storage costs on the results in the tables; for the water/steam and lithium/sodium/steam systems we have respectively

$$C_{H_2O} = \$71\ \mathrm{M} + [\$3.7\ \mathrm{M} \times t_{dw}(\mathrm{s})],$$

$$C_{Na} = \$32\ \mathrm{M} + [\$1.9\ \mathrm{M} \times t_{dw}(\mathrm{s})].$$

Examination of the cost of thermal storage for the two systems indicates that the costs for the liquid-lithium breeder is significantly lower. The primary reason for the lower cost of the liquid-metal system is due to low-pressure operation of the thermal storage system (1.5 MPa liquid-metal breeder versus 15 MPa for water-cooled solid breeder). It should be noted, however, that the liquid lithium blanket was studied in less detail; the increased costs of tritium containment (such

Table 2
Cost of thermal storage system [a]: water-cooled $Li_2O$ breeder

| | Basic cost | Cost of additional components for 10 s dwell |
|---|---|---|
| High pressure vessels (@ $14 M each) | 28 | 28 |
| Charging pumps | 10 | |
| Piping | 5 | 1 |
| Valves | 8 | |
| Condensate storage | 5 | 1 |
| Instrumentation and control | 5 | 1 |
| Building and structures (incremental) | 4 | 2 |
| Installation | 8 | 4 |
| Total | 71 | 37 |

[a] $M (1983).

Table 3
Cost of thermal storage system [a]: self-cooled lithium blanket

| | Basic unit | Cost of additional components for 10 s dwell |
|---|---|---|
| Storage vessels | 6.5 | 6.5 |
| Sodium charge | 0.3 | 0.3 |
| Piping | 3.6 | 1.8 |
| Valves | 7.1 | 4.0 |
| Building and structures (incremental) | 2.6 | 1.5 |
| Gas blanket and emergency venting | 1.2 | 0.6 |
| Sodium cleanup system | 2.0 | 0.6 |
| Instrumentation and control | 3.0 | 1.2 |
| Installation | 4.0 | 1.5 |
| Miscellaneous | 2.0 | 1.0 |
| Total | 32.3 | 19.0 |

[a] $M (1983).

as double-wall pipes), of heat exchangers (due to added thermal resistance of double-wall pipes), and of tritium cleanup and recovery systems have not been included in this analysis.

Although thermal energy storage is rather cheap ($\sim \$1.0 \times 10^{-3}$ to $\$5.0 \times 10^{-4}$ per joule) compared to electric energy storage, it appears to be a major cost item for pulsed burn cycles due to the tremendous energy storage required for long dwells. For a typical dwell of $t_{dw} = 30$ s this cost amounts to $\sim \$90$ M to $\sim \$180$ M, depending on which storage medium is selected. However, cost savings with shorter dwells may be negated by increased costs associated with the electric power supplies for pulsed burn cycles. The optimum dwell period depends on details of the burn cycle, which are discussed in ref. [6].

## 5. Conclusions

Our findings fall into different categories. In the area of operating goals and material properties we find:

- For any cycle with a fusion period as short as $\sim 1$ h there is a first wall and limiter life limit imposed by thermal fatigue, especially if there are frequent or severe disruptions. Thermal fatigue ceases to be a major concern if disruptions are very rare ($f \lesssim 10^{-4}$) or of low energy density ($\lesssim 200$ J/cm$^2$), if vapor shielding is significant, or if the melt layer is not lost from the affected surface. On the other hand, a single disruption could be fatal if it initiates cracks in the first wall which lead to premature thermal fatigue failure.
- Use of materials with superior thermal fatigue resistance may permit shorter fusion burns for a given replacement period of the reactor component. However, if structural materials such as vanadium are selected for their high radiation resistance, then there appears to be a need to extend burn lengths in order that thermal fatigue not prevent the achievement of longer in-reactor life. Considering the uncertainties surrounding disruption-induced damage, the full benefits of radiation resistant materials may only be guaranteed with the CW burn cycle.

Regarding issues of plasma physics we conclude:

- If very low plasma edge temperatures ($< 50$ eV) are possible then tungsten could serve as an ideal thin limiter leading edge coating with the result that disruptions and thermal fatigue would have negligible impact on the leading edge lifetime.
- Our understanding of what initiates disruptions must improve. If disruptions are eliminated by merely holding the toroidal current constant, then the IT and hybrid cycles can be attractive compared to the OH cycle. However, if density variations can also trigger disruptions then the CW cycle may be the only good alternative.

In this report we have considered only one subsystem (thermal storage) which has a large impact on the initial cost of a tokamak reactor, in the sense that its cost may vary significantly with the burn cycle (CW versus pulsed). Additional capital cost variations between burn cycles are presented in ref. [6]. However, we feel that the life limits for the first wall and limiter or divertor plates may crucially affect the attractiveness of tokamak reactors to electric utilities since the reliability of these components may have a strong impact on the overall power plant availability. Thus, long pulse operation ($t_f \lesssim 1$ h) may be the best guarantee of economical electrical generation.

## Acknowledgments

We wish to thank D.L. Smith and R.F. Mattas, who contributed significantly to our understanding of fusion materials problems.

This work was supported by the US Department of Energy.

## References

[1] C.C. Baker et al., Nucl. Engrg. Des. 63 (1981) 199; for complete report see C.C. Baker et al., STARFIRE – a commercial tokamak fusion power plant study, Argonne National Laboratory Report, ANL/FPP/80-1 (1980).
[2] N.J. Fisch, Operating tokamaks with steady-state toroidal current, Princeton Plasma Physics Laboratory Report, PPPL-1772 (1981).
[3] N.J. Fisch, in: Proc. 3rd Joint Varenna–Grenoble Intern. Symp. on Heating in Toroidal Plasmas, EUR7979EN, Vol. III (1982) p. 841.
[4] C.E. Singer and D.R. Mikkelsen, J. Fusion Energy 3 (1983) 13.
[5] R.A. Bolton et al., in: Proc. 3rd Top. Mtg. on Technology of Controlled Nuclear Fusion, CONF-780508, Vol. II (1978) p. 824.
[6] D.A. Ehst et al., A comparison of pulsed and steady-state reactor burn cycles – Part II: Magnet fatigue, power supplies, and cost analysis, Nucl. Engrg. Des./Fusion 2 (1984) 319–336.
[7] D.A. Ehst et al., Tokamak burn cycle study: a data base for comparing long pulse and steady-state power reactors, Argonne National Laboratory Report, ANL/FPP/TM-178 (1983).
[8] D.A. Ehst, et al., J. Fusion Energy 2 (1982) 83.

[9] N.J. Fisch, Phys. Rev. Lett. 41 (1978) 873.
[10] N.J. Fisch and C.F.F. Karney, Phys. Fluids 24 (1981) 27.
[11] N.J. Fisch and A.H. Boozer, Phys. Rev. Lett. 45 (1980) 720.
[12] M. Prokolab et al., Lower hybrid current drive and heating experiments at the 1-MW RF power level on Alcator C, presented at 11th European Conf. on Controlled Fusion and Plasma Physics, Aachen, West Germany, September 1983.
[13] R. Motley et al., in: Noninductive current drive in tokamaks, Proc. IAEA Technical Committee Meeting, Culham, England, CLM-CD, Vol. II (1983) p. 299.
[14] N.J. Fisch, Nucl. Fusion 21 (1981) 15.
[15] T. Ohkawa, Nucl. Fusion 10 (1970) 185.
[16] R.L. Reid et al., in: Proc. 8th Symp. on Engineering Problems of Fusion Research, Vol. I (1979) p. 427.
[17] J.N. Brooks and R.L. Kustom, Nucl. Technol. 46 (1979) 61.
[18] L. Bromberg, D.R. Cohn and J.E.C. Williams, J. Fusion Energy 3 (1983) 63.
[19] D.R. Mikkelsen and C.E. Singer, Nucl. Technol./Fusion 4 (1983) 237.
[20] US Contribution to the International Tokamak Reactor Phase 2A Workshop, USA FED-INTOR/82-1 (1982), Georgia Institute of Technology, Atlanta.
[21] D.L. Smith et al., Fusion reactor blanket/shield design study, Argonne National Laboratory Report, ANL/FPP/79-1 (1979) Chap. 7.
[22] R.F. Mattas and D.L. Smith, Nucl. Technol. 39 (1978) 186.
[23] R.F. Mattas, Fusion component lifetime analysis, Argonne National Laboratory Report, ANL/FPP/TM-160 (1982).
[24] A.M. Hassanein, G.L. Kulcinski and W.G. Wolfer, J. Nucl. Mater. 103/104 (1981) 321.
[25] J.N. Brooks, Nucl. Technol./Fusion 4 (1083) 33.
[26] G.A. Deis, in: Proc. 9th Symp. on Engineering Problems of Fusion Research, Vol. II (1981) p. 1783.
[27] C.H. Buchanan, Energy storage for tokamak reactor cycles, Princeton Plasma Physics Laboratory Report, PPPL-1511 (1979).